First-principles calculations of a robust two-dimensional boron honeycomb sandwiching a triangular molybdenum layer

Sheng-Yi Xie,[1] Xian-Bin Li,[1,*] Wei Quan Tian,[1,2] Nian-Ke Chen,[1] Xu-Lin Zhang,[1] Yeliang Wang,[3] Shengbai Zhang,[1,4,†] and Hong-Bo Sun[1,‡]

[1]*State Key Laboratory on Integrated Optoelectronics, College of Electronic Science and Engineering, Jilin University, Changchun 130012, China*

[2]*State Key Laboratory of Theoretical and Computational Chemistry, Institute of Theoretical Chemistry, Jilin University, Changchun 130012, China*

[3]*Beijing National Laboratory of Condensed Matter Physics, Institute of Physics, Chinese Academy of Sciences, Beijing 100190, China*

[4]*Department of Physics, Applied Physics, & Astronomy, Rensselaer Polytechnic Institute, Troy, New York 12180, USA*

(Received 30 April 2014; published 28 July 2014)

A graphenelike two-dimensional boron honeycomb is inherently prohibited due to its empty π valence band. Based on chemical intuition and first-principles calculations, we design a two-dimensional crystal MoB_4 with two graphenelike boron honeycombs sandwiching a triangular molybdenum layer. It has the attractive electronic structure of double Dirac cones near Fermi level with high Fermi velocity, which are contributed by the coupling of Mo d orbitals and B p_z orbitals. Such a metal stabilized boron honeycomb system could even have both superconductivity and ferromagnetism through appropriate selection of the metal layer, such as manganese. The unique electronic properties of these two-dimensional systems inspire broad interest in nanoelectronics.

DOI: 10.1103/PhysRevB.90.035447 PACS number(s): 61.46.−w, 68.65.−k, 73.22.−f

I. INTRODUCTION

Atomically thick two-dimensional (2D) materials have increasingly attracted great interest since the discovery of graphene [1–13]. The honeycomb structure of graphene has many excellent electronic properties, such as Dirac cones and ballistic transport. As an extended instance, boron nitride naturally favors the honeycomb structure due to the complementarities of the valence electrons of B (s^2p^1) and N (s^2p^3) to C (carbon, s^2p^2). While lacking one electron compared with C, B atoms alone become difficult to form into a 2D honeycomb structure, and some efforts have been made to achieve a 2D B sheet. B clusters with a quasiplanar structure were theoretically predicted by Boustani [14] and were then confirmed by experiments [15–17]. Single-walled boron nanotubes [18] and boron nanocones [19] were successfully synthesized in experiments. Theoretically, Tang and Ismail-Beigi [20] suggested a stable 2D boron sheet model with hexagonal holes embedded in a triangle lattice. This model was verified both by Wu *et al.* [21], with a global minima structure searing method, and by Piazza *et al.*, [22] in photoelectron spectroscopy experiment. Penev *et al.* [23] suggested that this 2D B sheet tends to form polymorphism. However, none of the theoretical and experimental papers suggest a pure 2D boron honeycomb sheet. Therefore, the inherent electronic characters of honeycomb like that in graphene, such as Dirac cones, are usually absent in these 2D boron systems.

Figure 1(a) shows an isolated boron honeycomb structure and its electronic band structure. Compared to that of graphene, a single layer of boron honeycomb also holds the π band with a Dirac cone. Yet the empty delocalized band leads to poor stability compared with that of carbon honeycomb, as indicated in Fig. 1(b), with a large imaginary vibration frequency. To stabilize a 2D pure B sheet, Tang and Ismail-Beigi proposed a hybrid system composed of boron triangle and hexagon motifs [20]. The balance of electron-excessive triangle and electron-deficient hexagon stabilizes the system. However, the strong covalent interaction in triangle motifs destroys the pure "noble blood" of honeycomb. Thus, the outstanding electronic properties of honeycomb, such as Dirac cones, are absent in such a hybrid system. In order to get more fascinating electronic properties within a honeycomb framework, a question is naturally raised: How can a boron honeycomb be stabilized while still keeping the inherent electronic characteristic of the honeycomb? In a metal-doped graphene system [24], some metals (bound with graphene) transfer electrons to graphene yet do not ruin the Dirac dispersion of graphene. Thus, herein we use a metal layer with excessive electrons to stabilize the B honeycomb in order to keep the electronic characteristic of the honeycomb, as shown in Fig. 1(c) and 1(d).

In this paper, based on first-principles calculations, a 2D crystal MoB_4 is proposed. In this structure, two boron honeycomb sheets are adhered with a "pie" layer of metal molybdenum, forming a "sandwich." Its stability is verified by the phonon modes calculation and *ab initio* high temperature molecular dynamics (HTMD). The 2D crystal retains the electronic characteristic of the boron honeycomb and displays an interesting property with double Dirac cones around its Fermi level, which indicates a potential superior transport property. Such a boron honeycomb system can modulate its electronic characters through suitable metal doping. For example, by replacing Mo with transition-metal manganese (Mn), strong electron-phonon coupling (EPC) and ferromagnetism could possibly coexist. The present findings provide us insights into the design and control of exotic electronic characteristics in these metal stabilized boron honeycomb systems.

*Corresponding author: lixianbin@jlu.edu.cn
†Corresponding author: zhangs9@rpi.edu
‡Corresponding author: hbsun@jlu.edu.cn

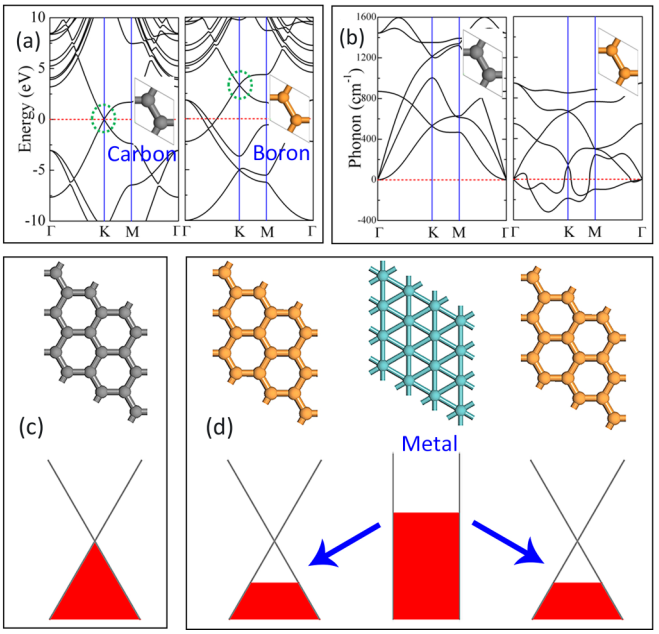

FIG. 1. (Color online) The sketch to stabilize B honeycomb. (a) Electronic band dispersion for graphene and B honeycomb. The insets are their atomic primitive cells. The dashed green ellipses mark their Dirac points. The Fermi level is set to the energy zero point. (b) Phonon frequency dispersion for graphene and B honeycomb. (c) graphene and its valence band occupation. (d) The sketch of stabilization for B honeycomb by metal. Gray, orange-yellow, and cyan balls represent C, B, and metal atoms, respectively.

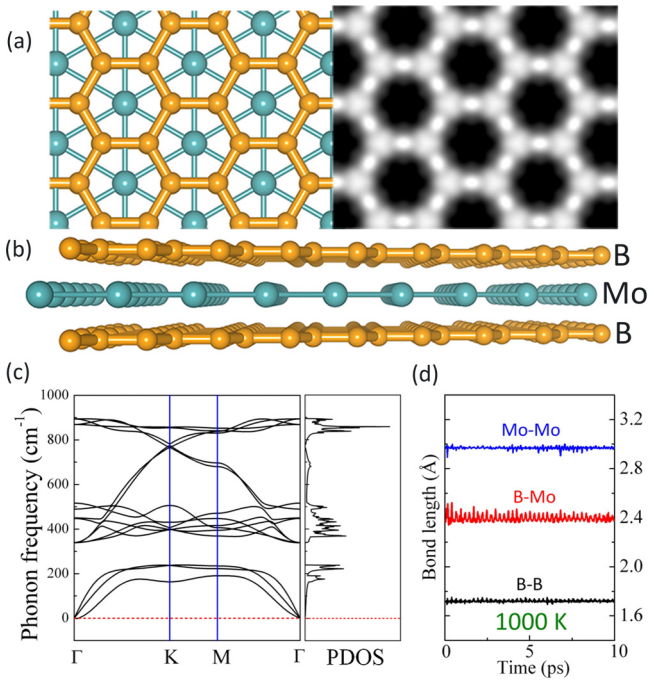

FIG. 2. (Color online) The structure and its stability for MoB_4. (a) Left is the top view of MoB_4, and right is corresponding STM image with a bias of −1.0 eV. (b) Side view of the structure. To show the structure clearly, the B-Mo bonds are not shown. (c) Phonon dispersion and PDOS of MoB_4. (d) Bond length evolution at 1000 K. Color coding of atoms is the same as in Fig. 1.

II. COMPUTATIONAL METHOD

A Perdew-Burke-Ernzerhof generalized gradient approximation based on density functional theory [25] was employed in the present paper, and the interactions between ion cores and valence electrons are described by the projector-augmented wave method [26], as implemented in the Vienna *Ab initio* Simulation Package code [27]. A vacuum layer of 15.4 Å is used to decouple interactions of neighboring slabs. A plane-wave cutoff of 450 eV and a Monkhorst-Pack 19 × 19 × 1 K-point mesh are taken for geometry optimization until all forces are smaller than 0.01 eV/Å. *Ab initio* HTMD is taken on the canonical ensemble [28], with a time step of 2 fs. During molecular dynamics, a (4 × 4) supercell, which contains 64 B and 16 Mo atoms, is used to relieve the constraint of the (1 × 1) cell. To get precise vibrational information, phonon modes and EPC were calculated within the framework of density-functional perturbation theory using the Quantum Espresso package [29]. A norm-conserving scheme was used to generate the psedopotentials for B, Mo, and Mn. A (6 × 6 × 1) q-point mesh in the first Brillouin zone was used in the EPC calculation. A dense grid of (12 × 12 × 1) was used to ensure k-point sampling convergence. Before the phonon and EPC calculations, the structures of MoB_4 and MnB_4 are fully relaxed through the Quantum Espresso code.

III. RESULTS AND DISCUSSIONS

To fully fill the π band of the honeycomb, every boron atom needs one more electron to achieve the s^2p^2 configuration. In other words, the boron atom should have a valence of −1. The recent discovery of the MoS_2 2D crystal [30–32] indicates that metal Mo has good compliance in a 2D system. Thus, the composition of Mo and B in our system naturally suggests a 1:4 ratio. A layer of trigonal Mo lattice, which can be seen from the (110) slice in bulk body-centered-cubic Mo, has a lattice match with the boron honeycomb layer. Figure 2(a) and 2(b) give the top view and side view, respectively, of the constructed structure, where the triangle lattice Mo atoms are located above the center of the boron honeycomb from the top view. The bond lengths are 1.71, 2.37, and 2.97 Å for B-B, B-Mo, and Mo-Mo, respectively. The corresponding bond length in an isolated boron honeycomb is 1.685 Å, in bulk AlB_2-type MoB_2 is 2.413 Å (B-Mo bond), and in bulk Mo is 2.725 Å. Such a 2D MoB_4 system retains the bonding character from corresponding bulk materials. Figure 2(a) also gives the simulated scanning tunneling microscopy (STM) images with a bias of −1.0 eV, from which the B honeycomb lattice and B-B bond connections are clearly visible.

Figure 2(c) gives the phonon dispersions and the corresponding phonon density of state (PDOS). It is clear that the acoustical branches and optical branches of its vibration are well separated with a frequency gap. Furthermore, the absence of any imaginary frequency strongly suggests that the structure is a local minimum in its energy landscape. *Ab initio* HTMD confirms its kinetic stability. Through 10-ps molecular dynamics at 1000 K, such a 2D MoB_4 system keeps quite intact without any lattice destruction, as shown in Fig. 3. Moreover, Fig. 2(d) depicts the evolution of average bond length during

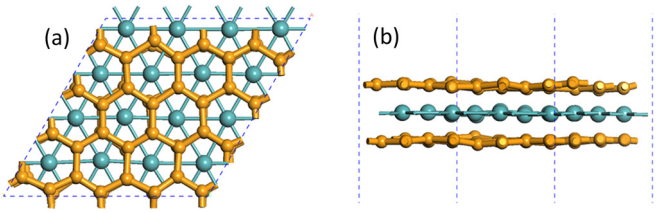

FIG. 3. (Color online) Snapshot of a (4 × 4) supercell of MoB_4 after 10 ps in HTMD kept at 1000 K. (a) Top view. (b) Side view. Color coding of atoms is the same as in Fig. 1.

the high temperature annealing. All B-B, B-Mo, and Mo-Mo bonds keep a small fluctuation around their center bond length, especially for B-B and Mo-Mo in the same plane.

The electron location function (ELF) [33] is utilized to analyze the bonding character in MoB_4. ELF can be described in the form of a contour plot in real space with values ranging from 0 to 1. The region with 1 indicates the strong covalent electrons or lone-pair electrons, the region close to 0 is typical for a low electron density area, and the region with 0.5 is an area with homogenous electron gas. Figure 4(a)–4(c) highlights the sliced planes containing B-B, Mo-Mo, and B-Mo bonds, respectively. Figure 4(d)–4(f) displays their corresponding ELF plots. In the connection between B atoms of the same plane, a high ELF distribution (∼0.9) centers on the middle of the bond, reflecting a strong covalent electron state with σ-like sp^2 hybridization like that in graphene [34]. In the connection between Mo and Mo, a 0.4 ELF extends all the space outside of the lattice, suggesting electronic "jellium" like that in metal. While in the connection between B and Mo, the ELF has significant contrast along the line indicating the form of ionic bonding. This is verified by the Bader charge analysis [35] that there is 1.0 electron of a Mo atom on average transferred to its neighboring B atoms. The filling of the π valence band of a boron honeycomb and Coulomb binding between Mo and B layers together leads to the stability in such a metal pinning boron honeycomb system.

The electronic properties including the band structure and the corresponding electronic densities of states (EDOS) are presented in Fig. 5(a)–5(c). At the energy window close to

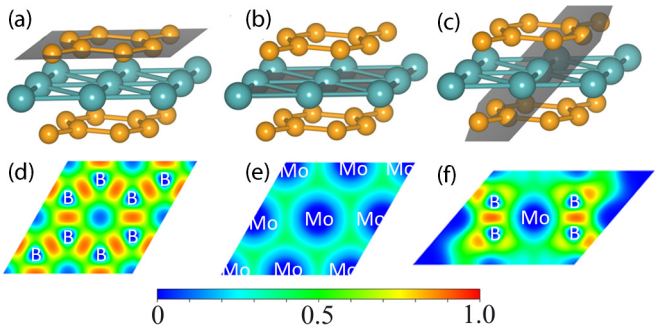

FIG. 4. (Color online) Bonding mechanism of MoB_4 reflected from ELF. (a)–(c) Cutting slabs along the B-B bond, Mo-Mo bond, and B-Mo bond plane, respectively. (d)–(f) Their corresponding ELF. For clarity, a (2 × 2) supercell is used here. Color coding of atoms is the same as in Fig. 1.

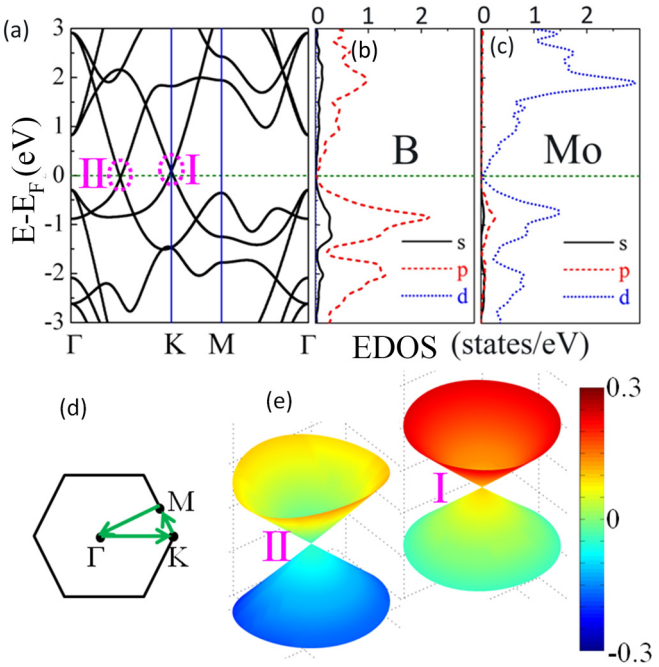

FIG. 5. (Color online) Electronic structure of MoB_4. (a) Band structure of MoB_4. The dashed pink ellipses indicate two Dirac cones, marked by I and II. (b) and (c) Projected EDOS for B and Mo atoms. (d) First Brillouin zone and high-symmetry points along band structure path for MoB_4. (e) 3D rendering of Dirac cones.

the Fermi level (from $E_F - 0.3$ eV to $E_F + 0.8$ eV), two Dirac cones come out. The high-symmetry cone located at K (cone I) is just 95 meV above the Fermi level, and the other low-symmetry one at the site along Γ to K (cone II) is 45 meV below the Fermi level. The two cones have almost the same slope with an electronic Fermi velocity of 5.31×10^5 m/s, around half of that in graphene [36]. Thus, the new system has an excellent electronic transport property. The site-projected EDOS shows the Dirac cone bands are composed mainly of the d electrons of Mo and the p electrons of B. Furthermore, the band-decomposed charge density for the two Dirac points is shown in Fig. 6. It is clearly demonstrated that the coupling states of Mo d orbital and B p_z orbital are the origin of the two Dirac cones. More specifically, cone I in the K point of the Brillouin zone is derived from the coupling of p_z orbital and d_{xz}/d_{yz} orbital, which can be deduced from the orbital shape in Fig. 6(a). Conversely, in Fig. 6(b), cone II at the site along Γ to K is from the coupling of the p_z orbital of B and the $d_z{}^2$ (or $d_{xy}/d_x{}^2{}_{-y}{}^2$) orbital of Mo. Also, the same orbital composition between up and down states in cone I indicates a fine symmetry of its electronic state in the Brillouin zone, which is similar to the Dirac cone at K in graphene. Yet for cone II, the significant contrast of orbital composition between the two degenerated states indicates a lower symmetry of the electronic state and therefore a location along Γ to K in the Brillouin zone. Thus, Dirac fermions are derived not only from the p_z orbital [1] or the d orbital [36] but also from the coupling of them, as demonstrated in the present paper. Moreover, the coupling of p electrons with different d orbitals can induce various exotic Dirac cones located at different positions in the Brillouin zone, which beyond the Dirac point of graphene

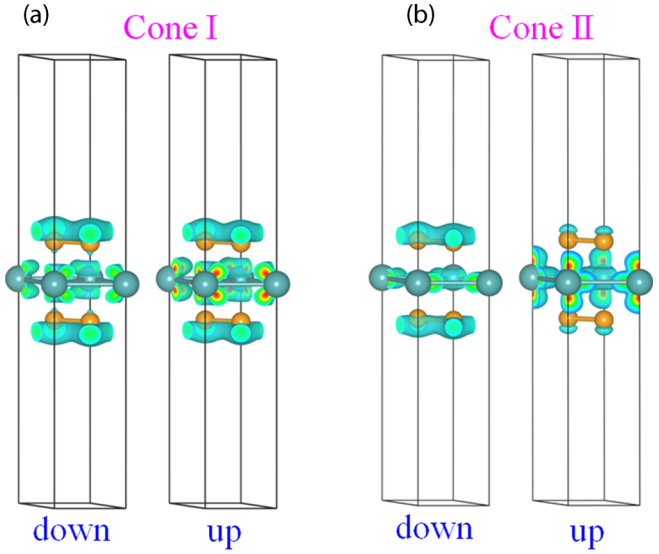

FIG. 6. (Color online) Charge density plots of states at Dirac points of MoB_4 with the isosurface value 0.01 e/a_0^3. The orbital distribution for Dirac points (a) I and (b) II in Fig. 5 is shown. Here, up and down are for the two crossing states in one cone.

merely contributed by the p_z orbital. The two Dirac cones in our paper are also different from the system of graphene bound with transition metal suggested by Li *et al.* [36]. Their Dirac cones derived mainly from graphene and transition metal separately are located at the same position K in the Brillouin zone but at different energy. However, in the present MoB_4, the two Dirac cones are at almost similar energy but are located at different positions in the Brillouin zone. The two Dirac cones, although with a large amount of d electrons, are still almost isotropic, as indicated by the three-dimensional (3D) plot in Fig. 5(e). If the effect of spin-orbit coupling is considered, the localized d electron of Mo can induce an energy gap of 38 and 55 meV for cone I and cone II, respectively, which is shown in Fig. 7. These gaps are much larger than graphene due to

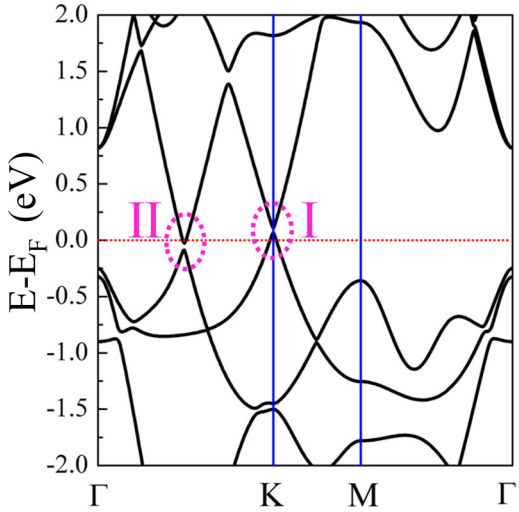

FIG. 7. (Color online) Spin orbit coupling opens the gap for the Dirac points in MoB_4 (38 meV for cone I and 55 meV for cone II). Fermi level is set at the energy zero point.

the large contribution of Mo d electrons in MoB_4 compared with the delocalized p_z orbital of graphene [37]. The energy band with two Dirac cones for 2D MoB_4 is quite similar to that with 6,6,12-graphyne, which indicates a good choice for a self-doping system [38].

Our proposed 2D MoB_4 can be produced in experiments. Bulk MoB_2 with the AlB_2 type structure, sequenced by stacking a boron honeycomb layer and a Mo triangle layer, can be stable under atmospheric conditions [39]. Furthermore, the boron honeycomb layer terminated MoB_2 (0001) surface is more stable than the Mo metal layer terminated MoB_2 (0001) surface [40]. Thus, with the molecular beam epitaxy technique to strictly control the layers of MoB_2, one may produce 2D MoB_4 by growing another B honeycomb layer on the Mo metal layer, which is supported by a B honeycomb layer on the bottom to form the sandwich structure. Thus, the suggested MoB_4 deserves an experimental trial to apply its exotic electronic properties in the future.

The 2D MoB_4 is in electronic balance in that its magnetic moment is zero. Magnetism may be produced by adding or decreasing electrons to break the balance. Mn, with five d electrons, has an extra electron compared with Mo. When replacing Mo with Mn in the same structure, as shown in the inset of Fig. 8(a), a ferromagnetic ground state for the 2D MnB_4 appears with a 1.64 μ_B/unit cell. Figure 8(a) also indicates that the magnetic EDOS, which is the difference for spin-up and spin-down EDOS, is mainly contributed by

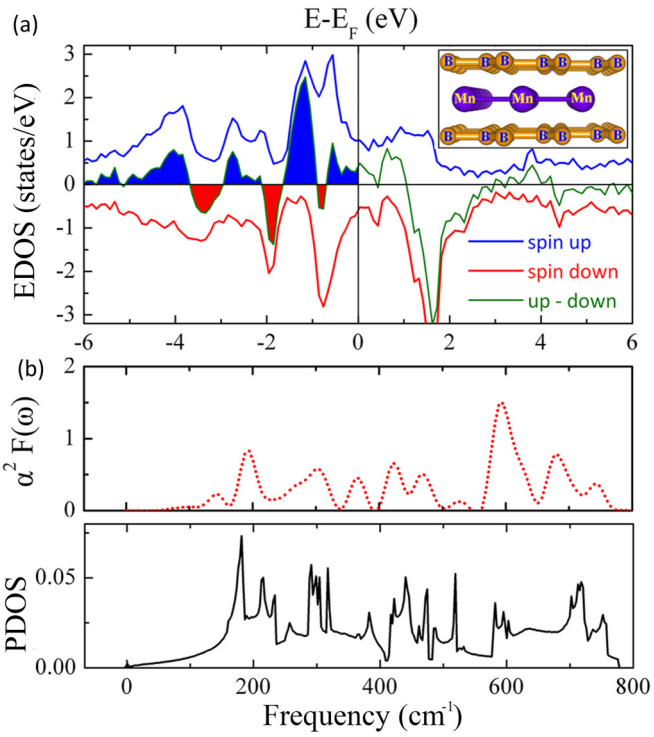

FIG. 8. (Color online) Ferromagnetism and superconductivity of MnB_4. (a) Spin-polarized EDOS for MnB_4. The blue line and the red line indicate spin-up and spin-down states, respectively, and the green line represents their difference (magnetic EDOS). The inset shows the corresponding structure obtained by replacing Mo with Mn. (b) PDOS and EPC Eliashberg function $[\alpha^2 F(\omega)]$ for MnB_4.

TABLE I. EPC-related parameters of MnB_4 in the conditions of spin-polarized calculation and non-spin-polarized calculation. The total coupling strength λ, the logarithmic average frequency (in Kelvins), and the superconducting transition temperature (T_c, in Kelvins) are estimated with the Coulomb parameter $\mu^* = 0.12$ according to the Allen-Dynes formula [48].

	λ	$\langle \log \omega \rangle$	T_c
Spin polarized	1.285	492.306 K	44.470 K
Non-spin polarized	0.494	291.057 K	2.416 K

the bands around −1.5 eV below the Fermi level. However, around the Fermi level, the total EDOS, which is the sum of spin-up and spin-down EDOS, is relatively large while the magnetic EDOS is small. This structure also holds strong electron-phonon interaction according to the framework of density-functional perturbation theory [41]. Its vibrational PDOS without imaginary frequency and the corresponding EPC parameters are calculated in Fig. 8(b). The large contribution for EPC is derived from the coupling between electrons and phonon modes around the frequency of 600 cm^{-1}. The total EPC parameter λ is 1.285, and the superconductivity critical temperature is estimated to be as large as 44.5 K, which is higher than the value of bulk MgB_2 [42,43]. Thus, this kind of structure may be a potential platform for applicable superconductors. The magnetism and superconductivity could coexist in this 2D system, which seems to be contradictory to the basic physical principles. According to the traditional Bardeen-Cooper-Schrieffer (BCS) theory [44], there is no magnetism in a conventional bulk superconductor due to the Meissner effect [45], which can screen the external magnetic field at the surface of a superconductor on a scale of hundreds of nanometers defined by the London penetration depth [46]. However, in the present 2D system, its atomic scale is far smaller than that of the conventional London penetration depth. In fact, the form of the Cooper pair needs opposite spin for the two electrons. Thus, the ferromagnetism will decrease the number of Cooper pairs. In the present system, the magnetism is mainly contributed by the states that lie well below the Fermi level, around the energy window of −5 to −4 and −2 to −1 eV, as shown in Fig. 8(a). Yet around the Fermi level, magnetic EDOS is not so significant as to completely cancel the formation of the Cooper pair. Further study finds that spin polarization increases the EPC largely compared with a non-spin-polarized situation (see Table I). Recently, Bazhirov and Cohen [47] suggested that static magnetic moments can induce significant enhancement of EPC in antiferromagnetic iron-based superconductors. Thus, future theoretical and experimental efforts should be made to fully understand the relation between magnetism and superconductivity in low-dimensional materials.

IV. CONCLUSION

We have successfully utilized a metal layer to stabilize a boron honeycomb. MoB_4, as the prototype of this sandwich structure, inherits the excellent electronic property of the honeycomb structure in which two Dirac cones appear around the Fermi level. The high Fermi velocity, with half of that for graphene, suggests that MoB_4 holds potential applications in low-dimensional, high-speed electronic devices. The 2D MnB_4 may be an interesting system in which ferromagnetism and superconductivity could coexist. Further effort, especially experiment synthesis, is urgently needed to realize not only the potential application in nanoelectronic devices but also the exploration of whether ferromagnetism and superconductivity can coexist in a 2D system.

ACKNOWLEDGMENTS

The present paper was supported by National Natural Science Foundation of China (Grants No. 11104109 and No. 11374119) and China Postdoctoral Science Foundation (Grant No. 2013T60315). W.Q.T. is grateful for support from the Open Project of State Key Laboratory of Supramolecular Structure and Materials (Grant No. SKLSSM201404). S.Z. is supported by U.S. Department of Energy Office of Basic Energy Sciences under Contract No. DE-SC0002623. The High Performance Computing Center at Jilin University is acknowledged for calculation resources.

[1] A. H. Castro Neto, N. M. R. Peres, K. S. Novoselov, and A. K. Geim, Rev. Mod. Phys. **81**, 109 (2009).
[2] M. Chhowalla, H. S. Shin, G. Eda, L. J. Li, K. P. Loh, and H. Zhang, Nat. Chem. **5**, 263 (2013).
[3] K. S. Novoselov, A. K. Geim, S. V. Morozov, D. Jiang, Y. Zhang, S. V. Dubonos, I. V. Grigorieva, and A. A. Firsov, Science **306**, 666 (2004).
[4] M. Xu, T. Liang, M. Shi, and H. Chen, Chem. Rev. **113**, 3766 (2013).
[5] L. Li, Y. Wang, S. Xie, X. B. Li, Y. Q. Wang, R. Wu, H. Sun, S. Zhang, and H. J. Gao, Nano Lett. **13**, 4671 (2013).
[6] M. Corso, W. Auwarter, M. Muntwiler, A. Tamai, T. Greber, and J. Osterwalder, Science **303**, 217 (2004).
[7] Y. Sun, Z. Sun, S. Gao, H. Cheng, Q. Liu, J. Piao, T. Yao, C. Wu, S. Hu, S. Wei *et al.*, Nat. Comm. **3**, 1057 (2012).
[8] P. Vogt, P. De Padova, C. Quaresima, J. Avila, E. Frantzeskakis, M. C. Asensio, A. Resta, B. Ealet, and G. Le Lay, Phys. Rev. Lett. **108**, 155501 (2012).
[9] L. Zhang, J. Yu, M. Yang, Q. Xie, H. Peng, and Z. Liu, Nat. Comm. **4**, 1443 (2013).
[10] S. Jungthawan, P. Reunchan, and S. Limpijumnong, Carbon **54**, 359 (2013).
[11] N. Papasimakis, S. Thongrattanasiri, N. I. Zheludev, and F. J. García de Abajo, Light Sci. Appl. **2**, e78 (2013).
[12] L. Wang, H. Y. Wang, Y. Wang, S. J. Zhu, Y. L. Zhang, J. H. Zhang, Q. D. Chen, W. Han, H. L. Xu, B. Yang *et al.*, Adv. Mater. **25**, 6539 (2013).
[13] S.-Y. Xie, X.-B. Li, Y. Y. Sun, Y.-L. Zhang, D. Han, W. Q. Tian, W.-Q. Wang, Y.-S. Zheng, S. B. Zhang, and H.-B. Sun, Carbon **52**, 122 (2013).
[14] I. Boustani, Surf. Sci. **370**, 355 (1997).

[15] H. J. Zhai, B. Kiran, J. Li, and L. S. Wang, Nat. Mater. **2**, 827 (2003).
[16] W. Huang, A. P. Sergeeva, H. J. Zhai, B. B. Averkiev, L. S. Wang, and A. I. Boldyrev, Nat. Chem. **2**, 202 (2010).
[17] A. N. Alexandrova, A. I. Boldyrev, H.-J. Zhai, and L.-S. Wang, Coord. Chem. Rev. **250**, 2811 (2006).
[18] F. Liu, C. Shen, Z. Su, X. Ding, S. Deng, J. Chen, N. Xu, and H. Gao, J. Mater. Chem. **20**, 2197 (2010).
[19] X. J. Wang, J. F. Tian, T. Z. Yang, L. H. Bao, C. Hui, F. Liu, C. M. Shen, N. S. Xu, and H. J. Gao, Adv. Mater. **19**, 4480 (2007).
[20] H. Tang and S. Ismail-Beigi, Phys. Rev. Lett. **99**, 115501 (2007).
[21] X. J. Wu, J. Dai, Y. Zhao, Z. W. Zhuo, J. L. Yang, and X. C. Zeng, ACS Nano **6**, 7443 (2012).
[22] Z. A. Piazza, H. S. Hu, W. L. Li, Y. F. Zhao, J. Li, and L. S. Wang, Nat. Comm. **5**, 3113 (2014).
[23] E. S. Penev, S. Bhowmick, A. Sadrzadeh, and B. I. Yakobson, Nano Lett. **12**, 2441 (2012).
[24] G. Giovannetti, P. A. Khomyakov, G. Brocks, V. M. Karpan, J. van den Brink, and P. J. Kelly, Phys. Rev. Lett. **101**, 026803 (2008).
[25] J. P. Perdew, K. Burke, and M. Ernzerhof, Phys. Rev. Lett. **77**, 3865 (1996).
[26] P. E. Blöchl, Phys. Rev. B **50**, 17953 (1994).
[27] G. Kresse and J. Furthmüller, Phys. Rev. B **54**, 11169 (1996).
[28] D. M. Bylander and L. Kleinman, Phys. Rev. B **46**, 13756 (1992).
[29] P. Giannozzi, S. Baroni, N. Bonini, M. Calandra, R. Car, C. Cavazzoni, D. Ceresoli, G. L. Chiarotti, M. Cococcioni, I. Dabo *et al.*, J. Phys.: Condens. Matter **21**, 395502 (2009).
[30] K. F. Mak, C. Lee, J. Hone, J. Shan, and T. F. Heinz, Phys. Rev. Lett. **105**, 136805 (2010).
[31] B. Radisavljevic, A. Radenovic, J. Brivio, V. Giacometti, and A. Kis, Nat. Nanotech. **6**, 147 (2011).
[32] J. N. Coleman, M. Lotya, A. O'Neill, S. D. Bergin, P. J. King, U. Khan, K. Young, A. Gaucher, S. De, R. J. Smith *et al.*, Science **331**, 568 (2011).
[33] A. Savin, O. Jepsen, J. Flad, O. K. Andersen, H. Preuss, and H. G. von Schnering, Angew. Chem. Int. Ed. **31**, 187 (1992).
[34] G. Gui, J. Li, and J. Zhong, Phys. Rev. B **78**, 075435 (2008).
[35] G. Henkelman, A. Arnaldsson, and H. Jónsson, Comp. Mater. Sci. **36**, 354 (2006).
[36] Y. Li, P. Chen, G. Zhou, J. Li, J. Wu, B.-L. Gu, S. B. Zhang, and W. Duan, Phys. Rev. Lett. **109**, 206802 (2012).
[37] M. Gmitra, S. Konschuh, C. Ertler, C. Ambrosch-Draxl, and J. Fabian, Phys. Rev. B **80**, 235431 (2009).
[38] D. Malko, C. Neiss, F. Vines, and A. Gorling, Phys. Rev. Lett. **108**, 086804 (2012).
[39] Q. Tao, X. Zhao, Y. Chen, J. Li, Q. Li, Y. Ma, J. Li, T. Cui, P. Zhu, and X. Wang, RSC Adv. **3**, 18317 (2013).
[40] N. Qin, S. Y. Liu, Z. Li, H. Zhao, and S. Wang, J. Phys.: Condens. Matter **23**, 225501 (2011).
[41] S. Baroni, S. de Gironcoli, A. Dal Corso, and P. Giannozzi, Rev. Mod. Phys. **73**, 515 (2001).
[42] J. Nagamatsu, N. Nakagawa, T. Muranaka, Y. Zenitani, and J. Akimitsu, Nature **410**, 63 (2001).
[43] H. J. Choi, D. Roundy, H. Sun, M. L. Cohen, and S. G. Louie, Nature **418**, 758 (2002).
[44] J. Bardeen, L. N. Cooper, and J. R. Schrieffer, Phys. Rev. **108**, 1175 (1957).
[45] W. Meissner and R. Ochsenfeld, Naturwissenschaften **21**, 787 (1933).
[46] F. London and H. London, Proc. R. Soc. London A **149**, 71 (1935).
[47] T. Bazhirov and M. L. Cohen, Phys. Rev. B **86**, 134517 (2012).
[48] P. B. Allen and R. C. Dynes, Phys. Rev. B **12**, 905 (1975).